Top-Down and Bottom-Up Diffusion of a Scalar in the Convective Boundary Layer

JOHN C. WYNGAARD AND RICHARD A. BROST[1]

National Center for Atmospheric Research,[2] Boulder, CO 80307

(Manuscript received 19 May 1983, in final form 29 August 1983)

ABSTRACT

The vertical diffusion of a passive, conservative scalar through the convective PBL is actually the superposition of what we call "top-down" and "bottom-up" processes. These component processes are driven by scalar fluxes at the mixed-layer top and bottom. We argue that the vertical asymmetry in the buoyant production of the turbulent kinetic energy should cause the top-down and bottom-up diffusivities to differ. If so, we show that the diffusivity for the total process is poorly behaved; it depends on the scalar flux profile and can have singularities.

We present results from large-eddy simulations which confirm that the top-down and bottom-up diffusivities are different, the latter being substantially larger. We present simple parameterizations for these diffusivities and the corresponding mean gradients. The results are useful in "unmixed-layer" models and in Fiedler's integral closure for scalar flux.

1. Introduction

The mean potential temperature Θ in the mid-portions of the planetary boundary layer (PBL) under clear-air, convective conditions is usually well-mixed (i.e., $d\Theta/dz = 0$). However, mean humidity mixing ratio (equivalently, mean specific humidity) Q, often is not. Mahrt (1976) has shown this clearly with the National Hail Research Experiment (NHRE) data from the high plains of the United States. Fig. 1, from Mahrt's paper, shows these Θ and Q data.

Mahrt pointed out, however, that in some cases moisture is also well-mixed. For example, he found that on clear days in the Wangara experiment the scaled dQ/dz values were much smaller than in the NHRE observations; Fig. 1 shows this.

Mahrt suggested that two processes could have caused the moisture gradients observed in NHRE: entrainment at the boundary-layer top and differential advection of moisture. He was unable to determine the exact cause, however. Nonetheless, Mahrt's paper raises an important question: What determines the vertical mean gradient of the mixing ratio of a scalar in the convective PBL?

In this paper we begin to answer this question. We consider dynamically passive scalars (i.e., those which do not influence the velocity field) which are also conservative (i.e., have no sources or sinks) and consider the clear-air, entraining, convective boundary layer under horizontally homogeneous conditions. Thus, we will not consider the second of Mahrt's mechanisms, differential advection, but this is often small anyway.

For this simplified case we find that entrainment can profoundly influence the mean scalar mixing ratio profile in the convective PBL through what we call "top-down" diffusion. We find further that this type of diffusion differs from the more familiar "bottom-up" type because of the vertical asymmetry of the buoyant forcing of the convective turbulence. We suggest that this difference between top-down and bottom-up diffusion is apt to be a fundamental property of buoyancy-driven turbulent layers.

2. Scalar transport in the convective PBL

Figure 2 is a representation of a convective PBL. As defined originally by Deardorff (1979), the interfacial layer at its top lies between the zero crossings of the potential temperature flux ($\overline{\theta w}$) profile. The broad mid-region of the PBL is called the mixed layer and below this is the surface layer. Since the definition of the surface layer is rather arbitrary, we take its thickness h_0 to be much less than the mixed-layer depth h_1. Thus the scalar flux at h_0 differs negligibly from that at the surface.

Consider a passive, conservative scalar whose ensemble mean mixing ratio C satisfies the conservation equation

$$\frac{\partial C}{\partial t} + U_i \frac{\partial C}{\partial x_i} + \frac{\partial}{\partial x_i} \overline{cu_i} = 0. \tag{1}$$

Here C, c, U_i and u_i are the mean and fluctuating scalar mixing ratio and wind velocity, respectively, and re-

[1] Present affiliation: Centre National Recherches Météorologiques, Avenue Eisenhower Prolongée, 31057 Toulouse Cedex, France.

[2] The National Center for Atmospheric Research is sponsored by the National Science Foundation.

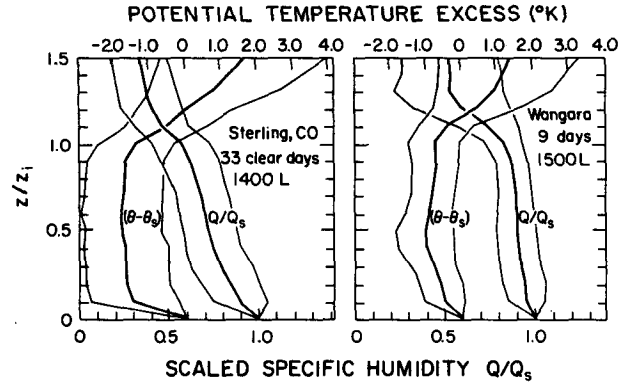

FIG. 1. Composite profiles of potential temperature and specific humidity from the NHRE (left) and Wangara (right) experiments. Thin lines represent standard deviations. Before averaging, specific humidity profiles were scaled with respect to the surface value, while the potential temperature profiles were reduced by the surface value. For NHRE, average z_i = 1710 m, average Q_s = 9.3 g kg^{-1}; for Wangara, average z_i = 915 m, average Q_s = 4.1 g kg^{-1}. From Mahrt (1976).

peated indices are summed. We assume that all components of the mean advection term in (1) and the horizontal components of the flux divergence term, are negligible compared to the vertical flux divergence. Thus the simplified form of (1) which we use is

$$\frac{\partial C}{\partial t} + \frac{\partial}{\partial z}\overline{cw} = 0, \tag{2}$$

where $u_i = (u, v, w)$ and $x_i = (x, y, z)$. We will call $\overline{cw}$ the scalar flux.

Writing (2) in the form

$$\frac{\partial}{\partial t}\frac{\partial C}{\partial z} + \frac{\partial^2}{\partial z^2}\overline{cw} = 0 \tag{3}$$

shows that in our simple situation, curvature in the scalar flux profile is caused only by time changes in the mean scalar gradient. If we assume for the moment that these changes are negligible (we return to this assumption later) then it follows that the $\overline{cw}$ profile is linear. If we denote the scalar flux at the surface by $\overline{cw_s}$ and that at mixed-layer top by $\overline{cw_1}$, then the scalar flux profile is

$$\overline{cw} = \overline{cw_s}(1 - z/h_1) + \overline{cw_1}(z/h_1). \tag{4}$$

Thus, the scalar flux profile has contributions from the surface flux (through bottom-up diffusion) and from the entrainment flux (through top-down diffusion). Fig. 3 shows schematically the profiles of mean scalar mixing ratio and scalar flux in our idealized convective PBL.

a. *Bottom-up diffusion*

Consider first a convective PBL undergoing purely bottom-up diffusion, that is, one with a scalar flux at the surface but zero flux at h_1 (see Fig. 4). For our idealized conditions, the flux in the mixed layer is

$$\overline{cw} = \overline{cw_s}(1 - z/h_1), \tag{5}$$

as sketched in the upper right panel of Fig. 4.

Now consider what parameters determine the mean scalar gradient $\partial C/\partial z$ within the mixed layer of our idealized PBL, given that we have only bottom-up diffusion. We assume that conditions are sufficiently convective that the friction velocity u_* is not important; a minimum group is then the surface scalar flux $\overline{cw_s}$, height z, mixed-layer depth h_1 and the convective velocity scale $w_* = (g\theta\overline{w_s}h_1/T)^{1/3}$. Dimensional analysis then implies that

$$\frac{\partial C}{\partial z} = \frac{-\overline{cw_s}}{w_* h_1} g_b, \tag{6}$$

where g_b (b for bottom-up) is the dimensionless gradient, a function of z/h_1.

The profiles of g_b and other quantities which we have sketched in Fig. 4 have some details which need explanation. For example, C does not decrease monotonically with z. It reaches a minimum near h_1 and then increases again; thus, g_b is negative in the interfacial layer. To show this, we integrate (2) between h_1 and h_2, using the fact that $\overline{cw}$ vanishes at these limits. In this way, we find that C conservation requires (Wyngaard and LeMone, 1980)

$$(h_2 - h_1)\frac{\partial C_1}{\partial t} = a_1 \frac{\partial h_1}{\partial t}(C_2 - C_1). \tag{7}$$

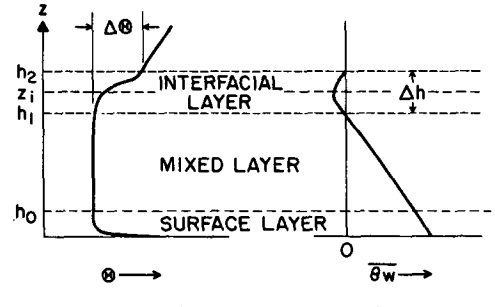

FIG. 2. A representation of a convective PBL, after Deardorff (1979).

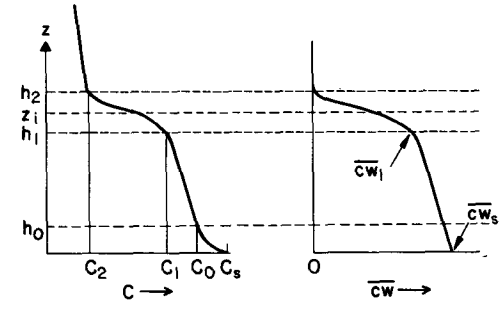

FIG. 3. The profiles of the mean (left) and vertical flux (right) of scalar mixing ratio in the convective PBL.

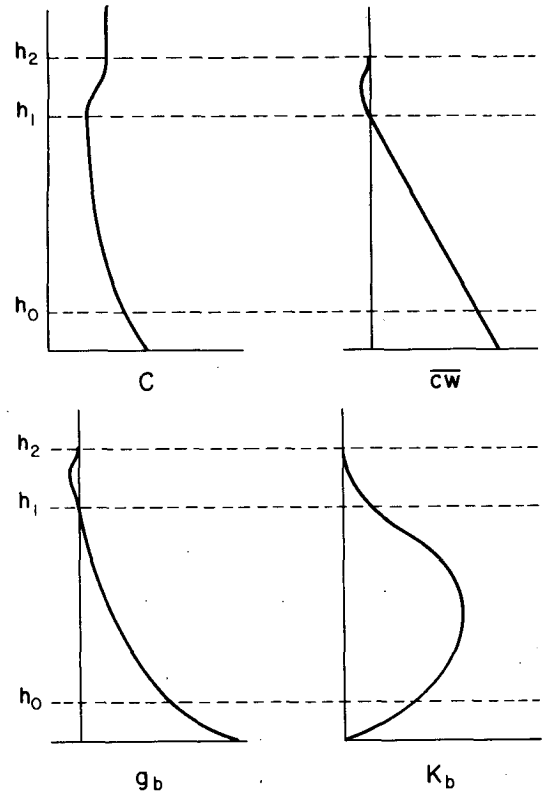

FIG. 4. Profiles in bottom-up diffusion: (upper left) mean mixing ratio; (upper right) scalar flux; (lower left) dimensionless mean gradient; (lower right) eddy diffusivity.

Here $a_1 \sim 1$ is a constant involving the shape of the C profile in the interfacial layer. Since from (2) $\partial C_1/\partial t$ is the negative of the scalar flux divergence at h_1, which is nonzero, then the left side of (7) is nonzero; thus, the right side of (7) requires $C_2 \neq C_1$. Inspection of (6) and (7) then shows that $\partial C/\partial z$ changes sign near h_1 and reaches zero again near h_2.

If we define an eddy diffusivity K in the usual way, then from (5) and (6) we have for bottom-up diffusion

$$K_b = \frac{-\overline{cw}}{\partial C_b/\partial z} = \frac{w_* h_1(1 - z/h_1)}{g_b}. \tag{8}$$

Note that K_b is singular near h_1 if the zero crossings of the flux and the gradient are not coincident. A well-behaved K_b is sketched in Fig. 4.

b. Top-down diffusion

Here there is a change in C across the interfacial layer but not across the surface layer (see Fig. 5). One can show (Lilly, 1968; Deardorff, 1979) that the entrainment-induced flux $\overline{cw_1}$ at the mixed-layer top (h_1) is

$$\overline{cw_1} \approx \frac{-\partial h_1}{\partial t}(C_2 - C_1). \tag{9}$$

Here the approximation sign becomes an equality as $h_2 - h_1$ approaches zero (Wyngaard and LeMone, 1980).

The parameters determining $\partial C/\partial z$ during top-down diffusion in our idealized mixed layer are, at a minimum, $\overline{cw_1}$, z, h_1 and w_*. It follows that

$$\frac{\partial C}{\partial z} = \frac{-\overline{cw_1}}{w_* h_1} g_t. \tag{10}$$

Note that we have given this dimensionless gradient function a subscript t for top-down. This immediately raises the question: Is $g_b = g_t$?

If conditions near the surface and near h_1 were symmetric (as in Raleigh–Benard convection between a heated lower surface and a cooled upper surface), then g_b and g_t would also be symmetric; i.e., $g_b(z/h_1) = g_t(1 - z/h_1)$. However, this is not the case in the convective PBL. The buoyant production rate of turbulent kinetic energy is proportional to the temperature flux profile, and as Fig. 2 shows, this is largest near the bottom. Thus, the strong convective plumes rising from the lower surface have no counterparts at the top; there the turbulence structure is different, with weakly turbulent, newly entrained fluid mixing with impinging convective eddies and broadly subsiding motions. We conclude that there is no reason to expect that the top-down and bottom-up diffusion processes are the same and thus we anticipate that g_b and g_t are also different. A sketch of a plausible g_t is shown in Fig. 5.

In the top-down case, the eddy diffusivity becomes

$$K_t = w_* z/g_t. \tag{11}$$

Again, if conditions at the mixed-layer top and bottom were symmetric, we would have $K_b(z/h_1) = K_t(1 - z/h_1)$, as inspection of (8) and (11) confirms. Because of the symmetric buoyant forcing, however, we expect that K_b and K_t could be quite different.

c. A superposition hypothesis

Consider a horizontally homogeneous, convective PBL. We assume it is quasi-steady, i.e., that the time changes in its governing parameters (e.g., surface fluxes, depth, entrainment parameters, mean pressure gradient) are sufficiently small that they do not directly affect the PBL structure and dynamics. Let the nonturbulent fluid above have a vertically uniform scalar mixing ratio and let this value be different from that typical of the boundary layer. Then the entrainment process generates a scalar flux at the mixed-layer top. We allow no scalar flux at the surface, so that only top-down diffusion takes place. Thus, we denote with a subscript t the scalar mixing ratio field which exists. The mean gradient field satisfies

$$\frac{\partial}{\partial t}\frac{\partial C_t}{\partial z} + \frac{\partial^2}{\partial z^2}\overline{c_t w} = 0, \tag{12}$$

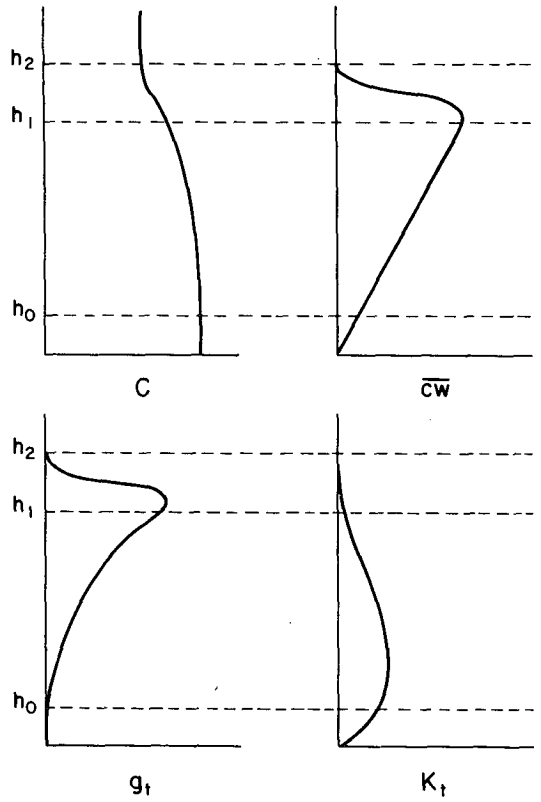

FIG. 5. As in Fig. 4, but for top-down diffusion.

and the flux boundary conditions are

$$\overline{c_t w} = 0 \quad \text{at} \quad z = 0; \quad \overline{c_t w} = F_1 \quad \text{at} \quad z = h_1. \tag{13}$$

Under these quasi-steady conditions and within the mixed layer, the scalar flux $\overline{c_t w}$ has a linear profile, the mean gradient $\partial C_t/\partial z$ is steady in time, and the fluctuating mixing ratio field c_t is statistically stationary. We assert that for a given PBL velocity field, the statistics of this top-down mixing ratio field are then uniquely determined.

Now assume that the scalar mixing ratio of the fluid above is, instead, just that required to drive the entrainment-induced scalar flux at h_1 to zero, as we discussed in conjunction with (7). We impose a scalar flux at the surface, so that we have only bottom-up diffusion. We label this scalar field with a subscript b, and have the mean equation

$$\frac{\partial}{\partial t}\frac{\partial C_b}{\partial z} + \frac{\partial^2}{\partial z^2}\overline{c_b w} = 0, \tag{14}$$

with the flux boundary conditions

$$\overline{c_b w} = F_s \quad \text{at} \quad z = 0; \quad \overline{c_b w} = 0 \quad \text{at} \quad z = h_1. \tag{15}$$

We assert that, again, the statistics of this bottom-up mixing ratio field are uniquely determined.

Now consider the sum of these two mixing ratio fields; i.e., let $C = C_t + C_b$, $c = c_t + c_b$. By adding (12) and (14), (13) and (15), we have, from the linearity of the mixing ratio equation (1), the mean equation

$$\frac{\partial}{\partial t}\frac{\partial C}{\partial z} + \frac{\partial^2}{\partial z^2}\overline{cw} = 0, \tag{16}$$

and the flux boundary conditions

$$\overline{cw} = F_s \quad \text{at} \quad z = 0; \quad \overline{cw} = F_1 \quad \text{at} \quad z = h_1. \tag{17}$$

We again assert that given the same velocity field the statistics of this total mixing ratio field are uniquely determined. Thus, they are given by $\partial C/\partial z = \partial C_t/\partial z + \partial C_b/\partial z$, $\overline{cw} = \overline{c_t w} + \overline{c_b w}$, $c = c_t + c_b$.

A simple physical example will clarify this superposition hypothesis. Imagine that a passive, conservative yellow dye is diffusing into the mixed layer from the bottom, with zero flux through the mixed-layer top. At the same time, a passive, conservative blue dye is diffusing in through the mixed-layer top, with zero flux at the bottom. Clearly the total dye concentration field is simply the sum of these two fields; i.e., the total dye flux is the sum of the yellow and blue fluxes, and the mean dye gradient is the sum of the mean yellow and blue gradients. If the two dyes are instead the same color, we have our superposition hypothesis.

d. The general case

Let us now return to the general case where the mixed layer has scalar fluxes at both top and bottom. We saw earlier, in Eq. (4), that the scalar flux profile is linear in our idealized case. The mean scalar gradient is, by our superposition argument, the sum of the component (i.e., the top-down and bottom-up) gradients; from (6) and (10) this gives

$$\frac{\partial C}{\partial z} = \frac{-(\overline{cw}_1 g_t + \overline{cw}_s g_b)}{w_* h_1}. \tag{18}$$

If the dimensionless gradients g_b and g_t are positive and if the scalar fluxes at bottom and top have the same sign, then (18) shows that their contributions to the total mean gradient are additive. This can lead to a relatively large mean mixing ratio gradient in the mixed layer, as often observed for humidity. If, on the other hand, the fluxes at bottom and top are of opposite sign (as with temperature) then (18) shows that the mean gradient can be much smaller or even zero. Thus (18) seems physical.

The eddy diffusivity K in the general case is, from (4) and (18),

$$K = \frac{-\overline{cw}}{\partial C/\partial z} = \frac{w_* h_1[\overline{cw}_s(1 - z/h_1) + \overline{cw}_1 z/h_1]}{g_b\overline{cw}_s + g_t\overline{cw}_1}$$

$$= \frac{K_b K_t \overline{cw}}{K_t\overline{cw}_s(1 - z/h_1) + K_b\overline{cw}_1 z/h_1}. \tag{19}$$

Note that g_b and g_t in (19) are, by definition, independent of the scalar fluxes at bottom and top. Thus, if these fluxes are such that the numerator vanishes but the denominator does not, then K is zero. If they are such that the denominator vanishes but the numerator does not, then K is infinite. Clearly, both can happen. Furthermore, note that, in general, K depends on the fluxes; thus, this K-closure is inherently nonlinear.

Some of this poor behavior of K has been known for some time through studies of temperature and has been interpreted as indicating the eddy-diffusivity concept is unphysical in the convective PBL. Indeed, we showed in the discussion after (8) that the bottom-up diffusivity K_b could have a singularity near the top of the mixed layer. However, we see from (19) that all of this can also happen when the top-down and bottom-up processes are perfectly well-behaved but simply have different diffusivity profiles.

We do not suggest that in practice it will be useful to decompose the C field into top-down and bottom-up components C_t and C_b to be treated separately. Using such a decomposition could be complicated, in view of the odd behavior of C_b sketched in Fig. 4. Rather, we introduced the decomposition as a conceptual tool, one which we feel makes our result (18) physically plausible. That result could have been obtained purely on dimensional grounds by assuming that $\partial C/\partial z$ in the mixed layer depends only on w_*, h_1 and the scalar fluxes at bottom and top. Without distinguishing the top-down and bottom-up diffusion processes, however, one might not have expected g_b and g_t to differ.

Up to this point we have rather arbitrarily used h_1 as the top of the mixed layer. While this was convenient for our purpose of illustrating the decomposition of scalar diffusion into bottom-up and top-down processes, we do not suggest that it is the optimum choice. In what follows, we will use the more familiar height z_i to scale our results.

3. Large-eddy simulations

a. Description of the model

We used large-eddy simulations to study top-down and bottom-up diffusion separately. R. Brost built a large-eddy model which is basically a dry version of that described by Deardorff (1980). We used 40 grid points in each of the three spatial directions, with the vertical grid interval $\Delta z = 50$ m and the horizontal intervals $\Delta x = \Delta y = 125$ m. To make the model description simpler, we will use Deardorff's notation in which $(\bar{u}, \bar{v}, \bar{w})$ is the resolvable velocity field, (u', v', w') is the unresolvable (subgrid) field and $\bar{E} = (\overline{u'^2} + \overline{v'^2} + \overline{w'^2})/2$ is the subgrid turbulence energy. The other notation is standard. The momentum equations are those given by Deardorff (1980):

$$\frac{\partial \bar{u}}{\partial t} = -\frac{\partial}{\partial x}\left(\bar{u}^2 + \overline{u'^2} - \frac{2}{3}\bar{E}\right) - \frac{\partial}{\partial y}(\bar{u}\bar{v} + \overline{u'v'}) - \frac{\partial}{\partial z}(\bar{u}\bar{w} + \overline{u'w'}) - \frac{\partial}{\partial x}\left(\frac{\bar{p}}{\rho_0} + \frac{2}{3}\bar{E}\right) + 2\Omega_z\bar{v} - 2\Omega_y\bar{w}, \quad (20)$$

$$\frac{\partial \bar{v}}{\partial t} = -\frac{\partial}{\partial x}(\bar{u}\bar{v} + \overline{u'v'}) - \frac{\partial}{\partial y}\left(\bar{v}^2 + \overline{v'^2} - \frac{2}{3}\bar{E}\right) - \frac{\partial}{\partial z}(\bar{v}\bar{w} + \overline{v'w'}) - \frac{\partial}{\partial y}\left(\frac{\bar{p}}{\rho_0} + \frac{2}{3}\bar{E}\right) - 2\Omega_z\bar{u}, \quad (21)$$

$$\frac{\partial \bar{w}}{\partial t} = -\frac{\partial}{\partial x}(\bar{u}\bar{w} + \overline{u'w'}) - \frac{\partial}{\partial y}(\bar{v}\bar{w} + \overline{v'w'}) - \frac{\partial}{\partial z}\left(\bar{w}^2 + \overline{w'^2} - \frac{2}{3}\bar{E} - \left\langle \bar{w}^2 + \overline{w'^2} - \frac{2}{3}\bar{E}\right\rangle\right) - \frac{\partial}{\partial z}\left(\frac{\bar{p}}{\rho_0} + \frac{2}{3}\bar{E} - \left\langle \frac{\bar{p}}{\rho_0} + \frac{2}{3}\bar{E}\right\rangle\right) + 2\Omega_y(\bar{u} - \langle\bar{u}\rangle) + \frac{g}{\theta_0}(\bar{\theta} - \langle\bar{\theta}\rangle). \quad (22)$$

Here the x axis points eastward and the y, northward. The overbars indicate an average over the grid volume, and primes indicate deviations from the local grid-volume average. The angular brackets $\langle\ \rangle$ denote an average over the horizontal plane. Note that (22) has the horizontally averaged hydrostatic and residual mean values subtracted to insure that $\langle d\bar{w}/dt\rangle = 0 = d\langle\bar{w}\rangle/dt = \langle\bar{w}\rangle$ with our cyclic boundary conditions. We chose a constant large-scale pressure gradient corresponding to a geostrophic wind of 5 m s^{-1} toward the east.

The conservation equations for potential temperature θ and scalar mixing ratio c are

$$\frac{\partial \bar{\theta}}{\partial t} = -\frac{\partial}{\partial x}(\bar{u}\bar{\theta} + \overline{u'\theta'}) - \frac{\partial}{\partial y}(\bar{v}\bar{\theta} + \overline{v'\theta'}) - \frac{\partial}{\partial z}(\bar{w}\bar{\theta} + \overline{w'\theta'}), \quad (23)$$

$$\frac{\partial \bar{c}}{\partial t} = -\frac{\partial}{\partial x}(\bar{u}\bar{c} + \overline{u'c'}) - \frac{\partial}{\partial y}(\bar{v}\bar{c} + \overline{v'c'}) - \frac{\partial}{\partial z}(\bar{w}\bar{c} + \overline{w'c'}). \quad (24)$$

The equation for subgrid turbulence kinetic energy $\bar{E}$ is

$$\frac{\partial \bar{E}}{\partial t} = -\frac{\partial}{\partial x_i}(\bar{u}_i\bar{E}) - \overline{u_i'u_j'}\frac{\partial \bar{u}_i}{\partial x_j} + \frac{g}{\theta_0}\overline{w'\theta'} - \frac{\partial}{\partial x_i}[\overline{u_i'(e' + p'/\rho_0)}] - \epsilon, \quad (25)$$

where $e' = (u'^2 + v'^2 + w'^2)/2$ and ϵ is the rate of dissipation within the grid volume. We parameterized ϵ, just as Deardorff, through

$$\epsilon = C\bar{E}^{3/2}/l, \tag{26}$$

where $C = 0.19 + 0.51l/\Delta S$, $\Delta S = (\Delta x \Delta y \Delta z)^{1/3}$ and l is the minimum of ΔS and

$$0.76\bar{E}^{1/2}\left(\frac{g}{\theta_0}\frac{\partial\bar{\theta}}{\partial z}\right)^{-1/2}.$$

Finally, we used Deardorff's parameterizations for the subgrid fluxes

$$\overline{u_i'u_j'} = -K_m\left(\frac{\partial\bar{u}_i}{\partial x_j} + \frac{\partial\bar{u}_j}{\partial x_i}\right) + \frac{2}{3}\delta_{ij}\bar{E}, \tag{27}$$

$$\overline{u_i'\theta'} = -K_h\frac{\partial\bar{\theta}}{\partial x_i}, \tag{28}$$

$$\overline{u_i'c'} = -K_h\frac{\partial\bar{c}}{\partial x_i}, \tag{29}$$

$$\overline{u_i'(e' + p'/\rho_0)} = -2K_m\frac{\partial\bar{E}}{\partial x_i}, \tag{30}$$

and for the subgrid eddy coefficients

$$K_m = 0.10l\bar{E}^{1/2}, \tag{31}$$

$$K_h = \left(1 + \frac{2l}{\Delta S}\right)K_m. \tag{32}$$

The principal difference between our model and that of Deardorff (1980) is the finite-difference scheme. For the spatial differencing of the advection terms, we followed Piacsek and Williams (1970); for the time differencing, we followed Klemp and Wilhelmson (1978) and used the leapfrog technique with an Asselin (1972) filter to suppress time splitting.

We used a horizontally homogeneous surface with a roughness length $z_0 = 0.01$ m and a uniform, specified temperature. The surface fluxes were found from the similarity relationships of Businger *et al.* (1971). Horizontal boundary conditions were periodic, and vertical boundary conditions were as in Deardorff (1980).

The top-down problem has a nonzero value of the scalar flux at mixed-layer top and a zero value at the bottom. The flux at the top was easily provided by starting the model with a change in $\bar{c}$ across the interfacial layer. To guarantee that the surface flux was zero, at the end of each time step $\bar{c}(x, y, 0)$ was set equal to the newly predicted value at the lowest interior grid point, $\bar{c}(x, y, \Delta z)$.

In the bottom-up problem, we maintained a surface flux by specifying a uniform value of $\bar{c}$ at the surface which was greater than the average $\bar{c}$ at $z = \Delta z$. In principle, we could then have obtained the bottom-up statistics in the following way. The simulation would begin with the initial scalar mixing ratio in the overlying free flow chosen to be larger than that in the PBL. Entrainment would then generate a negative scalar flux at h_1, but this would decrease in magnitude with time (due to the decreasing difference across the interfacial layer) and eventually pass through zero. A "snapshot" at the time of zero crossing would then provide one realization of the bottom-up field; averaging over an ensemble of these snapshots would produce the bottom-up statistics.

The difficulty with this technique, we discovered, is the large amount of computer time required to generate enough realizations to yield stable statistics. Thus, we used a much faster but approximate technique. We forced the flux to zero at mixed-layer top by setting, after each time step, the concentration above $z = z_t$ equal to the newly calculated value at z_t; thus, $\bar{c}(x, y, z > z_t) = \bar{c}(x, y, z_t)$. We chose z_t as 1350 m, the height of maximum scalar flux found in the top-down simulations. While this technique did not allow us to resolve the sign change in $\partial C_b/\partial z$ at the top, we believe it gave reliable results over most of the mixed layer.

For both bottom-up and top-down simulations, the model was integrated for about one hour in physical time before the data were collected and averaged. We averaged over the 5 km × 5 km horizontal planes and over 10 realizations, each 90s apart.

Figure 6 shows the resulting profile of potential temperature flux. Note that the subgrid-scale contribution is negligible except near the surface, and note also that $h_1 = 1250$ and $h_2 = 1550$ m; z_i, the height where $\overline{\theta w}$ reaches its negative maximum, is 1450 m. The convective velocity scale w_* (defined with z_i) was 1.25 m s^{-1} and the friction velocity u_* was 0.23 m s^{-1}; thus, z_i/L was −64, which indicates moderately strong convection.

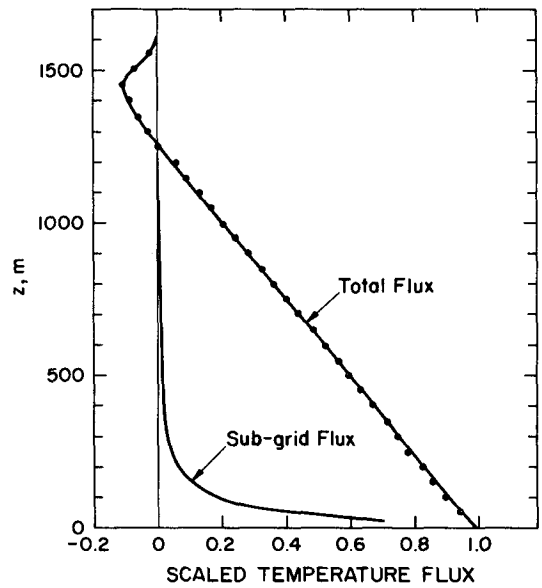

FIG. 6. Profiles of temperature flux (scaled with the surface value) from the large-eddy simulations.

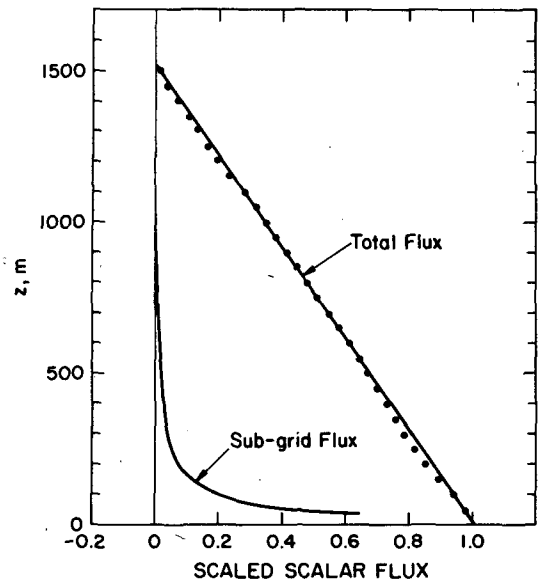

FIG. 7. Profiles of scalar flux (scaled with the surface value) from the large-eddy simulations.

b. Results

Figures 7 and 8 show the profiles of scalar flux obtained in our simulations. In each case we have scaled the flux with its boundary value. The subgrid-scale contribution to scalar flux is small except very near the surface in the bottom-up case.

While the bottom-up flux profile (Fig. 7) shows the predicted linear shape, the top-down profile (Fig. 8) is distinctly curved. Eq. (3) shows that this curvature is due to the time-varying $\partial C/\partial z$ caused by the slow deepening of the PBL. This growth by entrainment was difficult to determine accurately, but it was 2–4 cm s^{-1}.

Although we held the mean scalar gradient zero above 1350 m in the bottom-up case, Fig. 7 shows that the scalar flux did not vanish until about 1500 m. The small positive scalar flux between 1350 m and 1500 m was maintained by buoyant production and turbulent transport, but would not have existed had the mean gradient been as required by (7).

The corresponding mean-gradient results are plotted in Figs. 9 and 10. The bottom-up mean gradient (Fig. 9) is fit well by the formula

$$\frac{-z_i w_*}{\overline{cw_s}}\frac{\partial C_b}{\partial z} = 0.4\left(\frac{z}{z_i}\right)^{-3/2} \tag{33}$$

which ignores the sign change near z_i which we showed earlier was necessary. If we rewrite this in terms of surface-layer scales, we can compare its behavior near the surface with tower observations. Rescaling (33) and using the definitions of w_* and L gives

$$-\frac{ku_* z}{\overline{cw_s}}\frac{\partial C_b}{\partial z} = 0.1\left(\frac{-z}{L}\right)^{-1/2}\left(\frac{-z_i}{L}\right)^{1/6}. \tag{34}$$

The best observations of mean scalar gradients in the surface layer are those for potential temperature. It is worth noting that the (z/L) dependence in (34) is just that found in the Kansas measurements of the mean potential temperature gradient ϕ_h (Businger *et al.*, 1971). They found that in the unstable surface layer, at heights up to 32 m and for $0.3 < -z/L < 2$, a good fit was

$$\phi_h = -\frac{kzu_*}{\overline{\theta w_s}}\frac{\partial \theta}{\partial z} = a_2\left(\frac{-z}{L}\right)^{-1/2}, \tag{35}$$

with the constant a_2 between 0.20 and 0.25. A range of $(-z_i/L)$ values from ~60 to 250 would give our result (34) this range of variation in a_2. Although z_i was not measured in the Kansas experiments, in retrospect this seems a likely range for those data. Thus we conclude that our bottom-up mean gradient results are consistent with the Kansas surface-layer data.

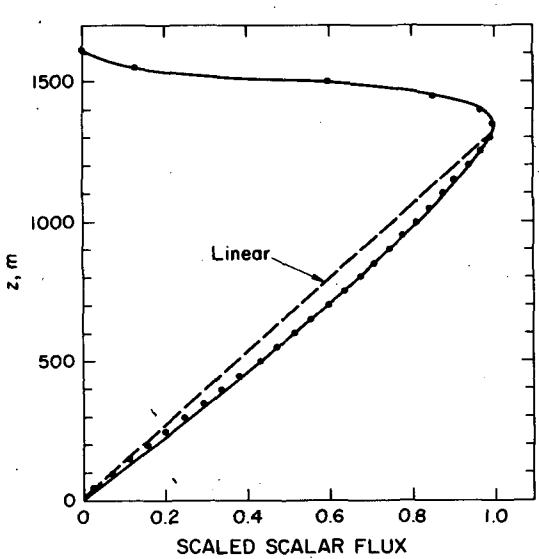

FIG. 8. The profile of scalar flux (scaled with the value at mixed-layer top) from the large-eddy simulations. The subgrid contribution was negligible.

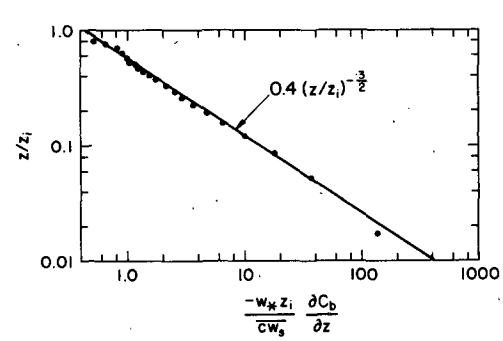

FIG. 9. The dimensionless mean gradient in bottom-up diffusion, from the large-eddy simulations.

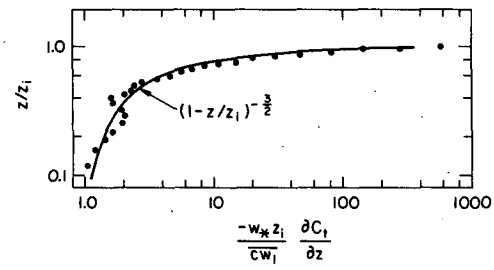

FIG. 10. The dimensionless mean gradient in top-bottom diffusion, from the large-eddy simulations.

Since in the logarithmic layer very near the surface the mean scalar gradient decreases as z^{-1}, at some height (say z_b) the mean gradient must break to the steeper $z^{-3/2}$ slope. We can estimate z_b by equating the gradients in the two regimes:

$$\left.\frac{\partial C}{\partial z}\right|_{z_b} \approx -0.74\,\frac{\overline{cw_s}}{ku_* z_b} \approx -0.4\,\frac{\overline{cw_s}}{z_i w_*}\left(\frac{z_b}{z_i}\right)^{-3/2}. \quad (36)$$

Solving for z_b gives

$$z_b \approx 0.036 z_i\left(\frac{u_*}{w_*}\right)^2, \quad (37)$$

which can also be written

$$z_b \approx 0.02 z_i^{1/3}(-L)^{2/3}. \quad (38)$$

If $z_i \sim 1000$ m and $-L = 10$ m, then (38) indicates $z_b \sim 1.0$ m. Thus, the break to $z^{-3/2}$ behavior would typically occur very close to the surface. Perhaps this is why the $z^{-4/3}$ regime predicted for "local free convection" is not observed and why instead, the surface-layer observations of $\partial\theta/\partial z$ under unstable conditions tend to fall as $z^{-3/2}$ even at the lowest observation heights (Businger *et al.*, 1971).

The top-down mean gradient g_t is plotted in Fig. 10. As discussed earlier, if conditions at mixed-layer top and bottom were symmetric then $g_t(z/z_i) = g_b(1 - z/z_i)$; it then follows from our bottom-up results (Fig. 9) that with symmetry, $g_t = 0.4(1 - z/z_i)^{-3/2}$. In fact, g_t is ~2.5 times larger than this, as Fig. 10 shows; a good fit to the data is

$$\frac{-z_i w_*}{\overline{cw_i}}\,\frac{\partial C_t}{\partial z} = \left(1 - \frac{z}{z_i}\right)^{-3/2}. \quad (39)$$

The scalar flux results (Figs. 7 and 8) and the mean gradient results (Figs. 9 and 10) imply the top-down and bottom-up eddy diffusivities shown in Fig. 11. The K_b results are fit well by

$$K_b = 2.5 w_* z_i\left(1 - \frac{z}{z_i}\right)\left(\frac{z}{z_i}\right)^{3/2}, \quad (40)$$

which follows from the K-definition (7), our formula (33) for the mean gradient, a linear flux profile and neglect of the difference between z_i and h_1. The corresponding formula for K_t is

$$K_t = w_* z\left(1 - \frac{z}{z_i}\right)^{3/2}. \quad (41)$$

Our results for K bring to mind those reported by Lamb and Durran (1978). Using data from large-eddy simulations of continuous point-source diffusion in the convective PBL, they found that K depends strongly on the source height z_s. The K profiles from the two source heights $z_s = 0.025 z_i$ and $z_s = 0.25 z_i$ are of opposite shape, but have comparable maximum values of the order of $0.25 w_* z_i$.

Figure 11 shows that the K_t formula (41) underpredicts the data at midlevels. Part of this is due to scatter in the mean gradient data in mid-regions (see Fig. 10) and part is due to the enhancement of scalar flux in midlevels caused by the flux profile curvature generated by the PBL growth.

We can now explain why this flux profile curvature is much more pronounced in the top-down case (Figs. 7 and 8). We start from (3) in the form

$$\frac{\partial^2 \overline{c_t w}}{\partial z^2} = \frac{\partial}{\partial t}\,\frac{\overline{c_t w}}{K_t}, \quad (42)$$

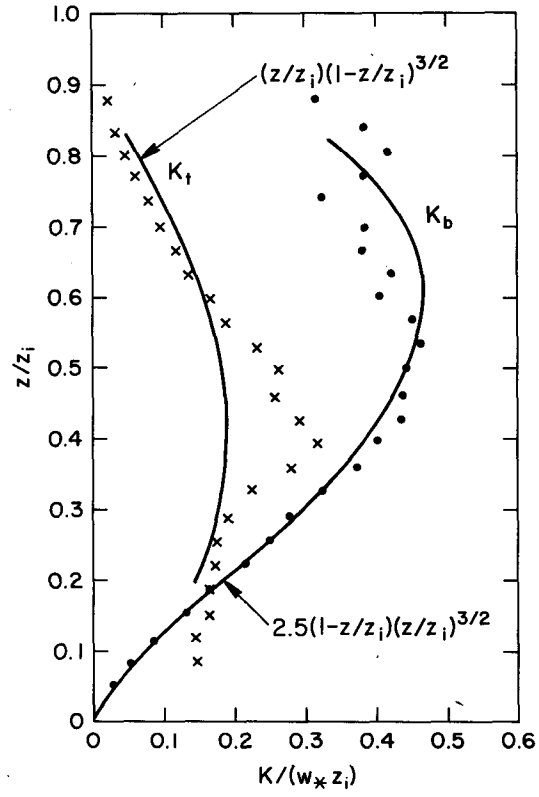

FIG. 11. Profiles of the top-down and bottom-up eddy diffusivities from the large-eddy simulations.

for the top-down case; the same expression, but with a subscript b, holds for bottom-up diffusion. Now we let the PBL depth z_i grow with time, but for simplicity we hold the other governing parameters (e.g., surface buoyancy flux, boundary scalar flux) constant. We scale the scalar flux with its boundary value F, and scale K with $w_* z_i$. Thus we write

$$\overline{c_t w} = F_t f_t\left(\frac{z}{z_i}\right),$$

$$K_t = w_* z_i D_t\left(\frac{z}{z_i}\right). \tag{43}$$

Using (43), the basic equation (3) becomes

$$\frac{\partial^2 f_t}{\partial\left(\frac{z}{z_i}\right)^2} = z_i^2 \frac{\partial}{\partial t}\left(\frac{f_t}{w_* z_i D_t}\right). \tag{44}$$

Carrying out the time differentiation in (44) and using $w_e = dz_i/dt$ in our subsidence-free case gives directly an expression for top-down flux profile curvature:

$$\frac{\partial^2 f_t}{\partial\left(\frac{z}{z_i}\right)^2} = \frac{-w_e}{w_* D_t}\left[\frac{z}{z_i}\frac{\partial f_t}{\partial\left(\frac{z}{z_i}\right)} + \frac{4}{3} f_t - \frac{z}{z_i}\frac{f_t}{D_t}\frac{\partial D_t}{\partial\left(\frac{z}{z_i}\right)}\right]. \tag{45}$$

The right side of (45) is w_e/w_* times a function of z/z_i. We can easily evaluate this function and its counterpart in the bottom-up case. In so doing we use, for example, $f_t \sim z/z_i$ and [from (41)] $D_t \sim (z/z_i)(1 - z/z_i)^{3/2}$. When we compare the results we find the curvature is much larger in the top-down case; the magnitude of the curvature ratio increases from 3 at $z/z_i = 0.2$ to 40 at $z/z_i = 0.5$ and 100 at $z/z_i = 0.8$. The flux profile calculated in this way are consistent with those in Figs. 7 and 8.

The formal solution to (45), using the boundary conditions at bottom and top, is simple, and shows that the difference in mid-PBL between the scaled flux and a linear profile is proportional to w_e/w_*. For our large-eddy simulations, $w_e/w_* \sim 0.03$ and the scaled flux difference (Δf) is $\sim$0.07 (Fig. 8); thus, $\Delta f \sim 2w_e/w_*$. It follows that in a rapidly growing PBL ($w_e/w_* \sim 0.05$–0.15), the mid-PBL departure from linearity could be 10–30% of the entrainment-induced flux. If the latter is not small compared to the surface flux, the scalar flux profile will be strongly curved.

The results (33), (39) and our superposition hypothesis imply that the mean scalar gradient in the mixed layer is

$$\frac{\partial C}{\partial z} = -0.4\frac{\overline{cw_s}}{z_i w_*}\left(\frac{z}{z_i}\right)^{-3/2} - \frac{\overline{cw_1}}{z_i w_*}\left(1 - \frac{z}{z_i}\right)^{-3/2}. \tag{46}$$

Integrating this over z gives for the C profile in the mixed layer,

$$C = 0.8\frac{\overline{cw_s}}{w_*}\left(\frac{z}{z_i}\right)^{-1/2} - 2.0\frac{\overline{cw_1}}{w_*}\left(1 - \frac{z}{z_i}\right)^{-1/2} + \text{constant}. \tag{47}$$

If we calculate the change ΔC across the mixed layer from (47), we obtain

$$\Delta C = -a'\frac{\overline{cw_s}}{w_*} - a''\frac{\overline{cw_1}}{w_*}, \tag{48}$$

where a' and a'' are constants. This is the form suggested by André *et al.* (1979) for water vapor mixing ratio changes across the mixed layer. Taking the mixed-layer bottom as $0.1z_i$ gives, from (47), $a' = 1.7$, the value also found by André *et al.* from their analysis of Wangara, AMTEX, Haswell, and Voves data. The constant a'' is more difficult to determine, both from our computer simulations and from observations. In the former case the problem is the strong increase in $\partial C_t/\partial z$ near z_i, which causes the value of a'' determined from (47) to depend on choice of the top of the mixed layer. From (47) we find $a'' = 4.3$ if the top is taken as $0.9z_i$, $a'' = 7$ for $0.95z_i$ and $a'' = 12$ for $0.98z_i$. André *et al.* suggest $a'' = 13$, within perhaps a factor of 2. Their determination of a'' has uncertainty introduced by considerable scatter in the measurements and also by their estimation of $\overline{cw_1}$ from an approximate entrainment relation rather than from direct flux measurements. We conclude, therefore, that our results are in reasonable agreement with the experimental findings of André *et al.*

Mahrt and André (1983) have parameterized the density gradient in the interior of an entraining boundary layer as the second term in our (48). They show data indicating that a'' is approximately 20 for two-layer salt-stratified flows and approximately 6 for linear-temperature stratified flows, although again there is considerable scatter.

Some C profiles calculated from (47) are shown in Fig. 12. Note that a "well-mixed" layer results for small negative values of $R = \overline{cw_1}/\overline{cw_s}$; the scalar flux can even become "countergradient," as routinely observed for potential temperature (Deardorff, 1966). Positive R values, on the other hand, give distinctly "unmixed" profiles. Note the similarity between the profiles in Fig. 12 and the corresponding ones in Fig. 1.

4. Application to the real PBL

a. *The impact of our idealizations*

The real PBL is continuously evolving in time. Let us examine how this affects the applicability of our quasi-steady results.

We saw that the component scalar diffusion processes can be described in terms of eddy diffusivities

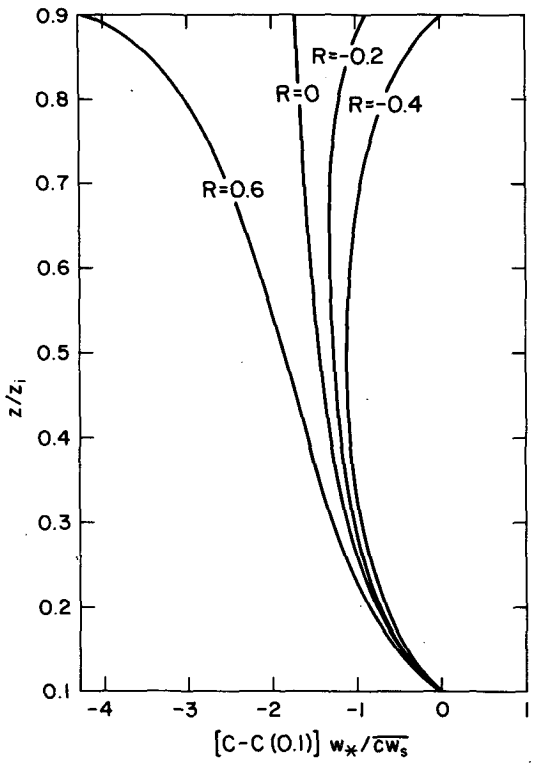

FIG. 12. Scaled mixing-ratio profiles calculated for four values of $R = \overline{cw}_1/\overline{cw}_s$. Negative R gives temperature-like profiles, positive R gives humidity-like profiles; compare with Fig. 1.

which scale with $w_* z_i$. Thus, as the PBL evolution changes the diffusion boundary conditions, the scalar field responds on a time scale of order $z_i^2/K \sim z_i/w_*$.

Consider now the time scale of the changes in the scalar boundary conditions. The scalar fluxes at mixed-layer top and bottom are proportional to the mean scalar jumps across the interfacial and surface layers respectively. If the changes in scalar mixing ratio at the surface and above the PBL are slow compared to the changes inside, then we can write for the time changes in these scalar jumps ΔC

$$\frac{\partial}{\partial t}\Delta C \approx -\frac{\partial}{\partial z}\overline{cw} \approx \frac{w_i \Delta C}{z_i}, \qquad (49)$$

where $w_i = w_e$ at the top and $w_i = ku_*/\ln(h_0/z_0)$ at the bottom. Thus, from (49) a time scale of the changes in ΔC, and hence in the scalar boundary fluxes, is z_i/w_i. Typically, $w_i \ll w_*$ so that the time scale of the changes in scalar fluxes at the boundaries is typically much greater than the response time of the scalar field within the PBL.

A similar calculation shows that away from the morning and evening transitions, the time scale of changes in surface buoyancy flux and z_i is also much greater than the response time of the internal scalar field. We conclude, therefore, that our quasi-steady assumption is not restrictive.

We have also neglected mean advection of the scalar. One can show through the general form of the mean scalar gradient equation (3) that advection causes curvature in the mean scalar profile. One can also show with scaling arguments, however, that under many conditions this curvature is quite small. Criteria for the negligibility of the advective terms include $Uz_i/(L_x w_*) \ll 1$, where L_x is the horizontal length scale of the changes in the mean scalar field and U is the mean horizontal wind; and $W/w_* \ll 1$, where W is mean vertical velocity. These do not seem restrictive in many applications.

We conclude, therefore, that our quasi-steady, locally homogeneous model has relevance to the real convective PBL.

b. *Two scalar-field closures*

We have found that the eddy diffusivity K for a passive, conservative scalar in the convective PBL can be very poorly behaved if both top-down and bottom-up diffusion are present. For the same velocity field it can vanish, go to infinity, or take on arbitrary values, depending on the scalar boundary conditions. What then can we use as an alternative to K-closure for the scalar field equations in larger-scale numerical models of the convective PBL?

The answer depends on the nature of the model. It might have only a few layers in the vertical, with its model equations obtained by integrating the governing equations over z; these are often called mixed-layer models because of their assumed flat profiles in the convective PBL. For applications to scalar transport we can now generalize this to an unmixed-layer model. For closure one needs only the mean scalar profile shape and the scalar fluxes at bottom and top of the mixed layer; thus, our result (47) and the standard entrainment and surface-layer formulas provide closure.

On the other hand, the model might have a number of levels within the PBL. Such models have traditionally used eddy diffusivities for their scalar fields, and we have stressed the deficiencies of this closure. An alternative is provided by the work of Fiedler (1984). He proposes the integral closure

$$\frac{\partial}{\partial z}\overline{cw} = \int_0^{h_1} R(z, z')[C(z) - C(z')]dz', \qquad (50)$$

where the function $R(z, z')$ represents the turbulent exchange between levels z and z'. He shows that if the transfer processes from z to z' and from z' to z are the same, then R is symmetric; i.e., $R(z, z') = R(z', z)$. In this case the top-down and bottom-top diffusivities are also symmetric. By introducing asymmetry into R, Fiedler is able to reproduce our top-down and bottom-up diffusion results.

Acknowledgments. We are grateful to D. Durran, B. Fiedler, D. Fitzjarrald, J. Klemp, D. Lilly and

R. Rotunno for valuable discussions during this research, and to D. Flaming for promptly and skillfully typing the manuscript. This work was partially supported by the U.S. Environmental Protection Agency under Interagency Agreement DW930144-01-0 but has not been subject to EPA review procedures.

REFERENCES

André, J. C., P. LaCarrere and L. J. Mahrt, 1979: Sur la distribution verticale de l'humidite dans une couche limite convective. *J. Rech. Atmos.*, **13,** 135–146.

Asselin, R., 1972: Frequency filter for time integrations. *Mon. Wea. Rev.*, **100,** 487–490.

Businger, J. A., J. C. Wyngaard, Y. Izumi and E. F. Bradley, 1971: Flux-profile relationships in the atmospheric surface layer. *J. Atmos. Sci.*, **28,** 181–189.

Deardorff, J. W., 1966: The counter-gradient heat flux in the lower atmosphere and in the laboratory. *J. Atmos. Sci.*, **23,** 503–506.

——, 1979: Prediction of convective mixed-layer entrainment for realistic capping inversion structure. *J. Atmos. Sci.*, **36,** 424–436.

——, 1980: Stratocumulus-capped mixed layers derived from a three-dimensional model. *Bound.-Layer Meteor.*, **18,** 495–527.

Fiedler, B., 1984: An integral closure model for the vertical turbulent flux of a scalar in a mixed layer. *J. Atmos. Sci.*, **41,** 92–101.

Klemp, J. B., and R. B. Wilhelmson, 1978: The simulation of three-dimensional convective storm dynamics. *J. Atmos. Sci.*, **35,** 1070–1096.

Lamb, R. G., and D. R. Durran, 1978: Eddy diffusivities derived from a numerical model of the convective planetary boundary layer. *Nuovo Cimento,* **1C,** 1–17.

Lilly, D. K., 1968: Models of cloud-topped mixed layers under a strong inversion. *Quart. J. Roy. Meteor. Soc.*, **94,** 292–309.

Mahrt, L., 1976: Mixed layer moisture structure. *Mon. Wea. Rev.*, **104,** 1403–1418.

——, and J. C. André, 1983: On the stratification of turbulent mixed layers. *J. Geophys. Res.*, **88,** 2662–2666.

Piacsek, S. K., and G. P. Williams, 1970: Conservation properties of convection difference schemes. *J. Comput. Phys.*, **6,** 392–405.

Wyngaard, J. C., and M. A. LeMone, 1980: Behavior of the refractive index structure parameter in the entraining convective boundary layer. *J. Atmos. Sci.*, **37,** 1573–1585.